ARTICLE INFORMATION

Received: 9 November 2012 | Revised: 26 February 2013 | Accepted: 5 March 2013

doi: 10.1259/bjr.20120570

Cite this article as:
Buchbender C, Hartung-Knemeyer V, Forsting M, Antoch G, Heusner TA. Positron emission tomography (PET) attenuation correction artefacts in PET/CT and PET/MRI. Br J Radiol 2013;86:20120570.

SHORT COMMUNICATION

Positron emission tomography (PET) attenuation correction artefacts in PET/CT and PET/MRI

[1,2]C BUCHBENDER, MD, [3]V HARTUNG-KNEMEYER, MD, [2]M FORSTING, MD, [1]G ANTOCH, MD and [1,2]T A HEUSNER, MD

[1]Department of Diagnostic and Interventional Radiology, Medical Faculty, University of Dusseldorf, Dusseldorf, Germany
[2]Department of Diagnostic and Interventional Radiology and Neuroradiology, Medical Faculty, University of Duisburg-Essen, Essen, Germany
[3]Department of Nuclear Medicine, Medical Faculty, University of Duisburg-Essen, Essen, Germany

Address correspondence to: Dr Christian Buchbender
E-mail: *Christian.buchbender@med.uni-duesseldorf.de*

Objective: To compare the effect of implanted medical materials on ^{18}F-fludeoxyglucose (^{18}F-FDG) positron emission tomography (PET)/MRI using a Dixon-based segmentation method for MRI-based attenuation correction (MRAC), PET/CT and CT-based attenuation-corrected PET (PET_{CTAC}).

Methods: 12 patients (8 males and 4 females; age 58±11 years) with implanted medical materials prospectively underwent whole-body ^{18}F-FDG PET/CT and PET/MRI. CT, MRI and MRAC maps as well as PET_{CTAC} and PET_{MRAC} images were reviewed for the presence of artefacts. Their morphology and effect on the estimation of the ^{18}F-FDG uptake (no effect, underestimation, overestimation compared with non-corrected images) were compared. In PET_{MRAC} images, a volume of interest was drawn in the area of the artefact and in a reference site (contralateral body part); the mean and maximum standardised uptake values (SUV_{mean}; SUV_{max}) were measured.

Results: Of 27 implanted materials (20 dental fillings, 3 injection ports, 3 hip prostheses and 1 sternal cerclage), 27 (100%) caused artefacts in CT, 19 (70%) in T_1 weighted MRI and 17 (63%) in MRAC maps. 20 (74%) caused a visual overestimation of the ^{18}F-FDG uptake in PET_{CTAC}, 2 (7%) caused an underestimation and 5 (19%) had no effect. In PET_{MRAC}, 19 (70%) caused

spherical extinctions and 8 (30%) had no effect. Mean values for SUV_{mean} and SUV_{max} were significantly decreased in artefact-harbouring sites ($p<0.001$).

Conclusion: Contrary to PET attenuation correction artefacts in PET/CT, which often show an overestimation of the ^{18}F-FDG uptake, MRAC artefacts owing to implanted medical materials in most cases cause an underestimation.

Advances in knowledge: Being aware of the morphology of artefacts owing to implanted medical materials avoids interpretation errors when reading PET/MRI.

Diagnostic imaging in combination with positron emission tomography (PET) requires adequate correction of detected γ-rays for the attenuation effect caused by different body tissues. In combined PET/CT, CT data provide opportune information on tissue density, which is rescaled to the annihilation emission energy and used for PET attenuation correction (AC) [1]. Implanted materials, *e.g.* dental or orthopaedic implants, are often present in patients and lead to artificial AC, resulting in overestimation or underestimation of tracer uptake in PET/CT studies [2–4]. The integration of PET and MRI into one imaging modality (PET/MRI) necessitated MRI-based attenuation correction (MRAC). MRAC relies on either automated pattern recognition of anatomical structures, discriminated by differences in pixel grey values in MR images (atlas-based MRAC method), or tissue classification, for example by using a Dixon-based in- and out-of-phase separation of fat and water (segmentation method) [5,6]. However, the quality of both MRAC methods depends on correct visualisation of the individual anatomy in the MRI source data used for MRAC. Also, in MRI, implanted medical materials cause various artefacts. In tissues adjacent to the foreign material, complete signal loss, signal pile-up, signal dislocation and geometric distortion have been described [7]. Using a Dixon-based MRAC with tissue segmentation for PET/MRI, we encountered severe artefacts owing to implanted medical materials. These artefacts are assumed to lead to bias in PET quantification, with potential impact on diagnostic and therapeutic decision-making. Thus, the purpose of this study was to assess the effect of implanted medical materials on Dixon-based MRAC, [^{18}F]-fludeoxyglucose (^{18}F-FDG) PET/MRI and to compare this effect with ^{18}F-FDG PET/CT.

PATIENTS AND METHODS

Patients

In 12 consecutive oncological patients [8 males and 4 females; age 58±11 years (mean ± standard deviation)] who underwent routine ^{18}F-FDG PET/CT for staging, PET/MRI was additionally performed on the same day. Table 1 provides a summary of the patient diagnoses. This study was performed in accordance with the regulations of the local ethics committee.

PET/CT imaging

Whole-body (WB) ^{18}F-FDG PET/CT scans were obtained on an mCT™ PET/CT scanner (Siemens Molecular Imaging, Hoffmann Estates, IL). Before imaging, patients fasted for at least 6 h. All patients had blood glucose levels below 150 mg dl^{-1} at the time of ^{18}F-FDG injection. 290±45 MBq of ^{18}F-FDG was intravenously injected 60 min before the scan. The CT scan was done with the following parameters. Caudocranial scan direction, field of view (FOV): skull base to upper thighs, 120 kV, automatic mA s^{-1} adjustment (Care Dose 4D™; Siemens Healthcare, Erlangen, Germany; preset: 210 mAs), 5-mm slice thickness, 5-mm increment and pitch 1. PET scan: three-dimensional (3D) mode, 2-min emission time per bed position (45% overlap), reconstruction according to the ordered-subsets expectation

Table 1. Summary of patients' diagnoses

Patient number	Diagnosis[a]
1	Urothelial carcinoma
2	Lung cancer
3	Thymic cancer
4	Non-Hodgkin lymphoma
5	Lung cancer
6	Sarcoma
7	Renal carcinoma
8	Melanoma
9	Cancer of unknown primary
10	Colorectal carcinoma
11	Renal carcinoma
12	Breast cancer

[a]As clinically suspected.

maximisation (OSEM) algorithm with four iterations and eight subsets, 3D Gaussian filter: 4.0 mm full width at half maximum (FWHM); scatter correction.

Positron emission tomography/MRI

WB ^{18}F-FDG PET/MRI was performed on a Magnetom Biograph mMR™ (Siemens Healthcare). The PET/MRI consists of a 3-T MR scanner and an inline PET component equipped with a combination of lutetium oxyorthosilicate crystal and avalanche photodiode detectors. PET/MRI was performed following ^{18}F-FDG PET/CT with a mean delay from tracer injection of 131± 35 min. Imaging was performed in the caudocranial direction. The FOV contained the body volume from the head to the thighs. PET acquisition time was 8 min per bed position. PET images were reconstructed using the iterative algorithm OSEM, 3 iterations and 21 subsets, Gaussian filter: FWHM 4.0 mm; scatter correction. A dedicated mMR head and neck coil and, depending on the patient's height, up to four mMR body flex coils were used for MRI. MRI was performed simultaneously for PET imaging using the following sequence protocol for each bed position: coronal 3D volumetric interpolated breath-hold examination (VIBE) sequence [repetition time (TR) 3.6 ms, echo time 1 (TE_1) 1.23 ms, TE_2 2.46 ms, 3.12-mm slice thickness, FOV 500 mm] for Dixon-based AC; transverse T_1 weighted turbo-fast angle low shot (FLASH) sequence (TR 1800 ms, TE 2.05 ms, matrix size 320, 7.5-mm slices, FOV 450 mm). PET/MRI image fusion was performed for the transverse T_1 weighted turbo-FLASH images.

Image analysis

Qualitative analysis

One radiologist and one nuclear medicine physician performed image reading in consensus. CT images, MR images and MRAC maps were assessed for the presence of artefacts caused by implanted medical materials. Multiple dental implants or alloys within one denture quadrant were referred to as one. For evaluation, implanted medical materials were first identified on plain transverse CT images. Then the corresponding CT-based attenuation-corrected (CTAC) PET images (PET_{CTAC}) and MRAC PET images (PET_{MRAC}) were identified in comparison with the corresponding non-AC (NAC) PET images (PET_{CTNAC}, PET_{MRNAC}) followed by an evaluation of the implanted material's effect on the MRAC maps and T_1 weighted FLASH images. The resulting effect on the estimation of the ^{18}F-FDG-uptake in the artefact-harbouring area in PET_{CTAC} and PET_{MRAC} was rated as follows: (a) no effect on the estimation of the ^{18}F-FDG uptake, (b) underestimation of the ^{18}F-FDG uptake and (c) overestimation of the ^{18}F-FDG uptake. The effects of artefacts caused by implanted medical materials in PET_{CTAC} and PET_{MRAC} were then compared.

Quantitative analysis

Additionally, in the PET_{MRAC} images, a 3D spherical 2-cm^3 volume of interest (VOI) was drawn in each artefact site (VOI_{art}) as well as in an anatomically matched reference site (*e.g.* contralateral body part; VOI_{ref}). For each VOI, the mean and maximum standardised uptake values (SUV_{mean}, SUV_{max}) were noted. The effect of artificial MRAC (ΔSUV_{MRAC}) was calculated using Equation (1):

$$\Delta SUV_{MRAC} \equiv SUV_{(VOI_{ref})} - SUV_{(VOI_{art})}. \quad (1)$$

Statistics

The Kolmogorov–Smirnov test was performed to test for a normal distribution of SUV_{max} and SUV_{mean} values. Since data were normally distributed, a Student *t*-test for matched pairs was applied to test for differences in SUV_{max} and SUV_{mean} between VOI_{art} and VOI_{ref}. $p<0.05$ was considered to be statistically significant.

RESULTS

27 implanted medical materials were found. The types of materials are listed in Table 2, which also provides a summary of the image findings.

Qualitative analysis

Artefacts in CT and T_1 weighted FLASH MRI

All 27 implanted materials (100%) caused CT artefacts, and 19 (70%) led to artefacts in the T_1 weighted FLASH MR images. CT artefacts consisted of a mixture of "black and white streak" artefacts (Figure 1a). MR artefacts comprised a large zone of signal loss and smaller zones of signal pile-up (Figure 1b).

Artefacts in MRAC maps

17 out of 27 (63%) implanted medical materials caused artefacts in the MRAC maps. MRAC artefacts predominantly consisted of spherically shaped zones of tissue misclassified as "air", which were located around the implanted materials (Figures 1 and 2). In addition, the body surface over these artefacts was not detected correctly, resulting in an artificial connection between the area of tissue misclassification and the background

Table 2. Summary of the types of implanted medical materials, presence of artefacts in positron emission tomography (PET)/MRI and PET/CT and their effects on the estimation of ^{18}F-fludeoxyglucose (^{18}F-FDG) PET uptake based on qualitative assessment

Patient number	Implanted device type	Presence of artefact			Effect on [^{18}F]-FDG uptake estimation	
		CT	MRI	MRAC	PET_{CTAC}	PET_{MRAC}
1	Dental	+	+	−	↓	↓
2	Dental	+	+	+	↑	↓
4	Dental	+	−	−	−	−
4	Dental	+	−	−	−	−
5	Dental	+	+	+	↑	↓
5	Dental	+	−	−	↑	−
6	Dental	+	−	−	↑	−
6	Dental	+	+	+	↑	↓
7	Dental	+	+	+	↑	↓
7	Dental	+	+	+	↑	↓
8	Dental	+	+	+	↑	↓
8	Dental	+	−	−	↑	−
9	Dental	+	−	−	↑	−
9	Dental	+	−	−	↑	−
10	Dental	+	+	+	↑	↓
11	Dental	+	+	+	↑	↓
11	Dental	+	+	+	↑	↓
11	Dental	+	−	−	−	−
12	Dental	+	+	+	↑	↓
12	Dental	+	+	+	↑	↓
1	Injection port	+	+	+	↑	↓
5	Injection port	+	+	+	↓	↓
6	Injection port	+	+	−	↑	↓
11	Hip prosthesis	+	+	+	↑	↓
11	Hip prosthesis	+	+	+	↑	↓
12	Hip prosthesis	+	+	+	↑	↓
8	Sternal cerclage	+	+	+	↑	↓

MRAC, MRI-based attenuation correction; PET_{CTAC}, CT-based attenuation-corrected PET; PET_{MRAC}, MR-based attenuation-corrected PET.
+, yes; −, no; ↓, underestimation of [^{18}F]-FDG uptake; ↑, overestimation of [^{18}F]-FDG uptake.

(Figures 1 and 2). Out of nine patients with bilateral dental implants, four showed bilateral MRAC artefacts, three had unilateral and two no MRAC artefacts.

Artefacts in PET_{CTAC} and PET_{MRAC}

20 out of 27 (74%) implanted medical materials led to a visual streak and spot-like overestimation of the ^{18}F-FDG uptake in PET_{CTAC} (Figures 1 and 2), 2 led to a visual underestimation and 5 had no effect.

19 out of 27 (70%) implanted medical materials resulted in a large spherical-shaped underestimation of ^{18}F-FDG uptake in the PET_{MRAC} images (Figures 1 and 2); 8 had no effect on the PET_{MRAC} images. All

Figure 1. Transverse CT image (a) showing a typical artefact caused by a dental implant. The corresponding CT-based attenuation-corrected positron emission tomography (PET) (b) and PET/CT (c) images show an (artificially) increased ^{18}F-fludeoxyglucose (^{18}F-FDG) uptake (arrow in Figure 1b) of the adjacent soft tissue. The MRI-based attenuation correction (MRAC) map of the same patient (d) shows a large region of missing data and tissue misclassification as air around the dental implants, resulting in an artificially decreased ^{18}F-FDG uptake (arrow in Figure 1e) in the corresponding MRAC PET (e). The PET/MRI image (f) shows a severe artefact in the transverse T_1 weighted sequence used for anatomical correlation.

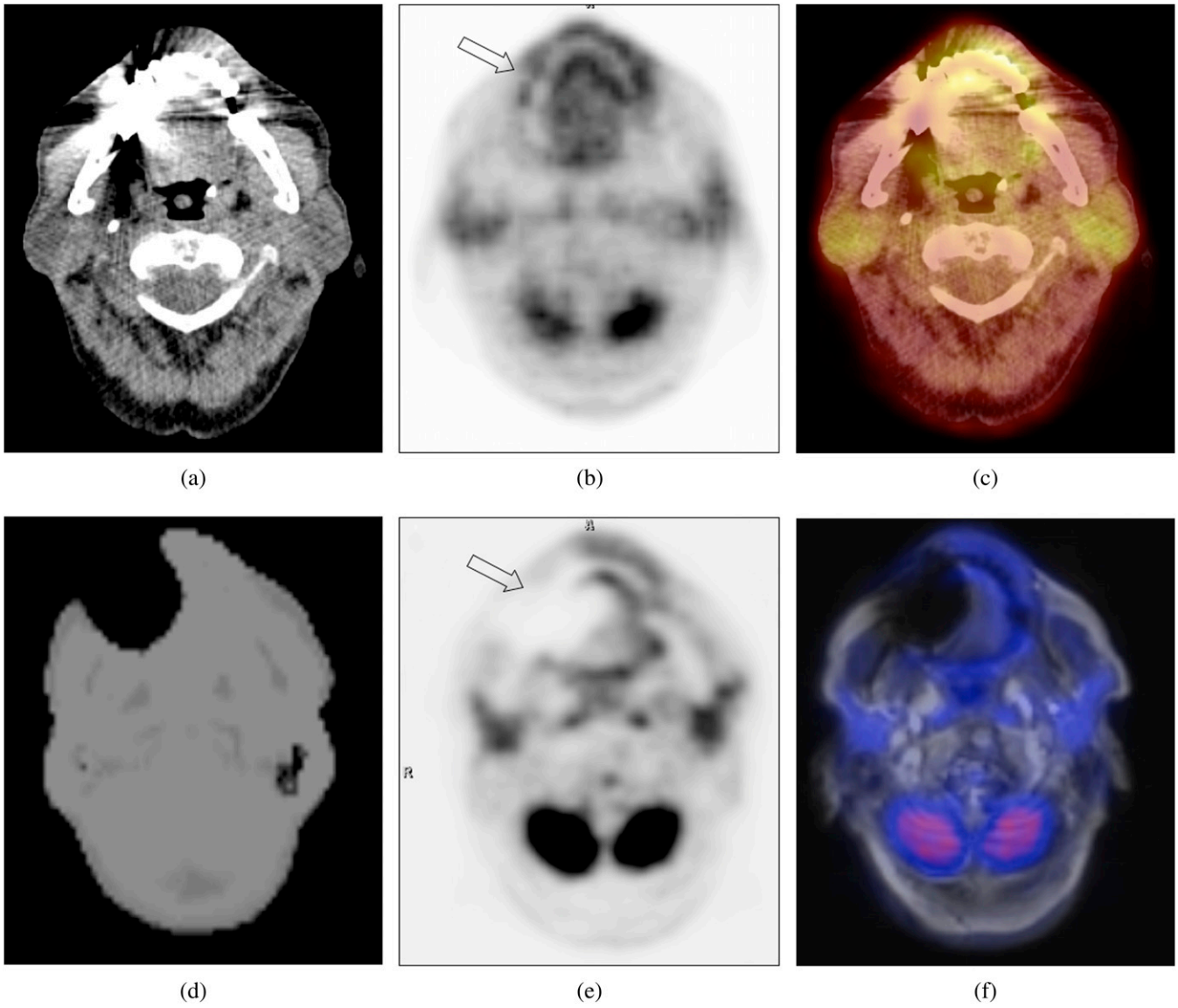

MRAC map artefacts resulted in an underestimation of ^{18}F-FDG uptake in the PET_{MRAC} images. In one case, an identical PET_{MRAC} artefact was found despite the absence of an MRAC map artefact. Out of 19 cases with artefacts in both PET_{CTAC} and PET_{MRAC}, 2 (11%) concordantly led to an underestimation of the ^{18}F-FDG uptake and 17 (90%) were discordant, showing an overestimation of the ^{18}F-FDG upatake in the PET_{CTAC} and an underestimation in the corresponding PET_{MRAC} images.

Quantitative analysis

The mean values for SUV_{mean} and SUV_{max} were significantly lower for VOI_{art} than the corresponding values for VOI_{ref} (0.046 ± 0.070 *vs* 0.420 ± 0.217; 0.126 ± 0.114 *vs* 0.647 ± 0.324; $p<0.001$) (Figure 3) with a mean $\Delta SUV_{mean_{MRAC}}$ of 0.374 ± 0.208 and a mean $\Delta SUV_{max_{MRAC}}$ of 0.520 ± 0.320. In one site with artificial MRAC, SUV_{mean} and SUV_{max} increased by 82% and 92%, respectively, owing to misclassification of fat as soft tissue. Excluding this single site, the SUV_{mean} and SUV_{max} of

Figure 2. Transverse CT image (a) showing a severe artefact caused by a hip prosthesis. The ^{18}F-fludeoxyglucose (^{18}F-FDG) uptake is (artificially) increased (arrow in Figure 2b) in the corresponding CT-based attenuation-corrected positron emission tomography (PET) (b) and PET/CT (c) images. The MRI-based attenuation correction (MRAC) map of the same patient (d) shows a region of missing data and tissue misclassification as air in the artefact-harbouring area, resulting in an artificially decreased ^{18}F-FDG uptake (arrow in Figure 2e) in the corresponding MRAC PET. (e) A severe artefact is shown in the transverse PET/MR image using a T_1 weighted sequence (f).

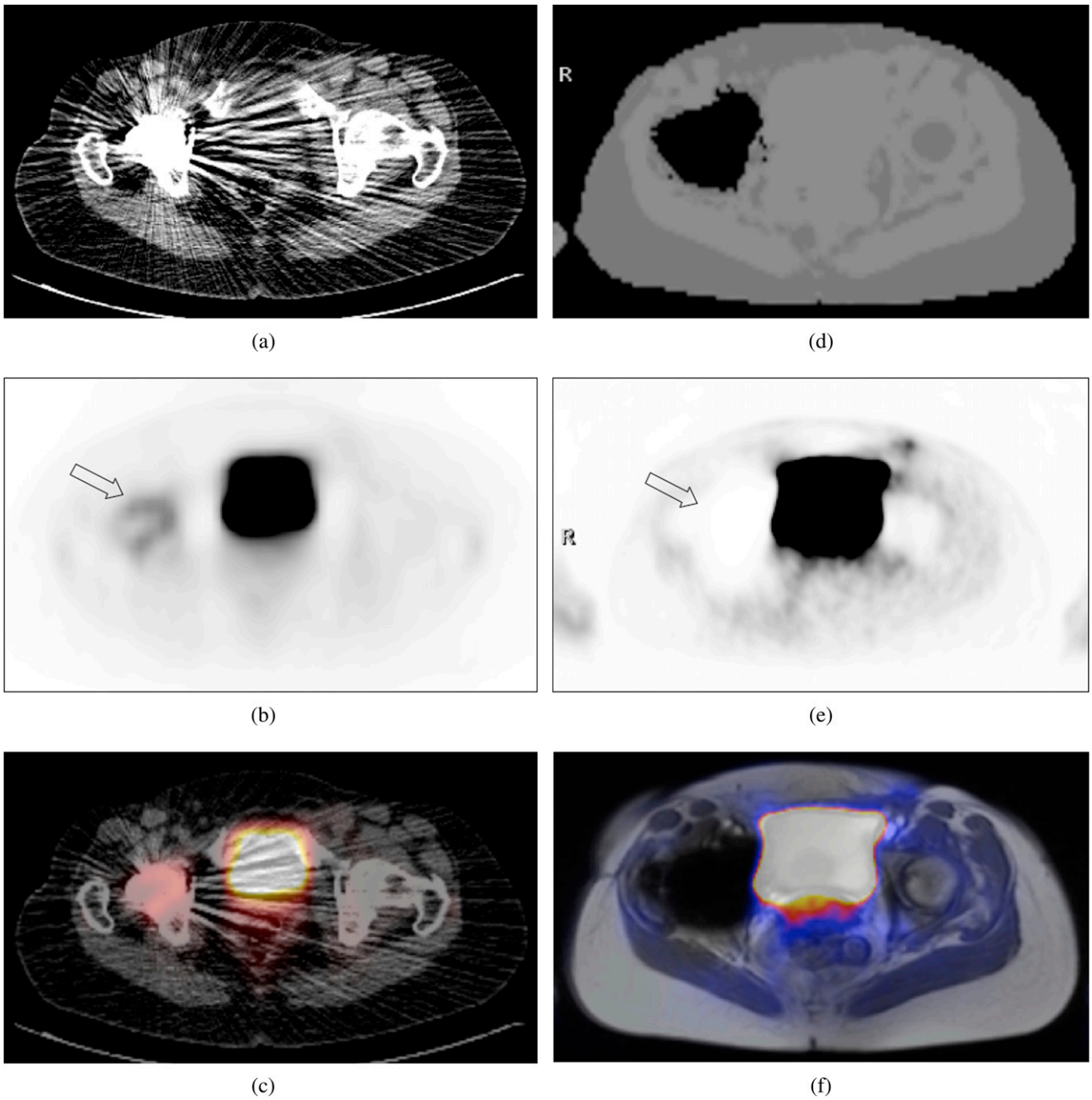

MRAC artefact-harbouring sites showed an average decrease of 93±11% and 84±14%, respectively.

DISCUSSION

AC is required for PET quantification in hybrid imaging modalities. The AC process has been described to be susceptible to artefacts caused by various factors, resulting in PET quantification errors. We present an initial comparative evaluation of the effect of CTAC and MRAC artefacts caused by implanted medical materials in a hybrid WB PET/MRI scanner on ^{18}F-FDG uptake estimation in PET_{CTAC} and PET_{MRAC}. We found that

Figure 3. Dot plots demonstrating a comparison of (a) the maximum (SUVmax) and (b) the mean standardised uptake values (SUVmean) in artefact harbouring sites and anatomical matched reference sites measured in the MRI-based attenuation-corrected positron emission tomography images.

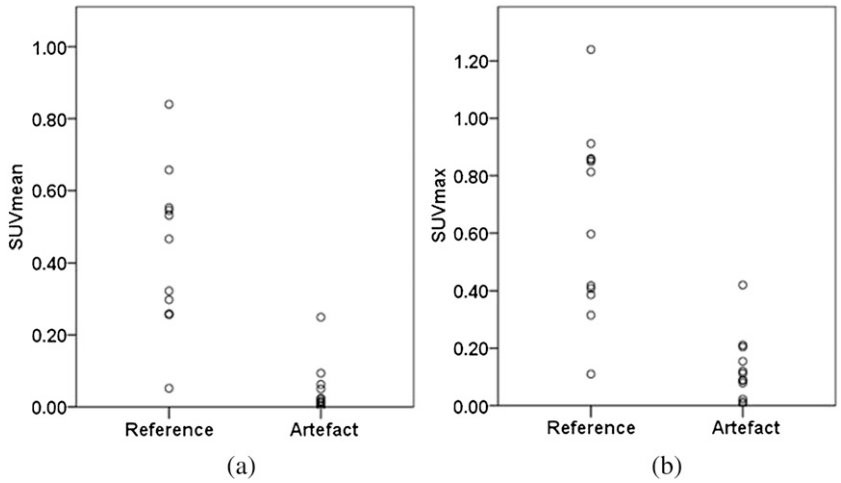

implanted medical materials led to a mixture of "dark streak" and "starburst" artefacts on CT images. Former PET/CT studies have demonstrated that these artefacts in CTAC cause two general types of quantification errors. "Dark streak" zones cause signal loss and consequently lead to an underestimation of the SUV [8]. The starburst artefact causes an artificial increase of the SUV, which has been identified as the predominant and clinically relevant effect for PET/CT reading [3]. In support, we also found that overestimation of the ^{18}F-FDG uptake in PET_{CTAC} was the predominant effect caused by implanted medical materials. Using a Dixon-based MRAC method, we found that implanted medical materials induced aberration of the local magnetic field and led to a spherical signal loss of the adjacent tissue, resulting in a misclassification as air instead of fat, soft tissue or bone in MRAC maps. Consequently, ^{18}F-FDG uptake of the artefact-harbouring area was greatly reduced in PET_{MRAC} images, and we found that the mean values for the SUV_{mean} and SUV_{max} in these sites were significantly decreased when compared with an individual reference site of the contralateral body. 90% of the sites with artefacts in both CTAC and MRAC showed discordant effects on the resulting PET images. Although the tracer uptake near the implanted medical material is overestimated in PET/CT [9,10], in most cases, it is substantially underestimated in regions harbouring MRAC artefacts. In a single case, in which the fat around an implanted subcutaneous injection port had been falsely classified as soft tissue, we found the SUV_{mean} and SUV_{max} increased by 82% and 92%, respectively. This exceptional finding demonstrates that the information provided by the MRAC maps can be relevant for PET/MR reading.

The fact that all implanted medical materials caused CT artefacts but only roughly 60% of the materials caused MRI and MRAC artefacts led to the question "what kind of specific material induces such artefacts?" Moreover, we did not experience any difference in the type of resulting artefacts between different types of implanted materials but we did not perform a systematic analysis of this. These questions will have to be answered for a reasonable allocation of patients to PET/CT and PET/MRI. For example, head and neck cancer patients with dental implants made from a material that induces severe PET/CT artefacts but less or no PET/MRI artefacts might benefit from a PET/MRI scan in terms of local staging and vice versa. Studies on CT, PET/CT and conventional MRI in patients with cancer of the oral cavity have shown that artefacts owing to dental implants can significantly impair the diagnostic quality of MRI [11]. In the same study, PET has been reported to be of great diagnostic value for the detection of oral malignancies, especially in CT studies that were affected by severe artefacts arising from the dental implants. Analogously, in PET/MRI, the uncorrected PET images might contribute to diagnostic information in areas that are affected by signal loss owing to dental implants and enable the detection of pathologies within these artefact-harbouring areas. For other oncological applications of PET/MRI, such as

PET quantification for therapy response assessment, the reported artefacts are currently disabled because quantification cannot be performed in NAC PET images.

For the choice of proper MRAC and diagnostic MRI protocols in PET/MRI, more information on the artefact susceptibility of the different sequences used for MRAC is required. The VIBE sequence we used for Dixon-based MRAC belongs to the gradient echo pulse sequence family, a technique that increases the susceptibility for the kinds of artefacts we reported in this study [12]. For conventional MRI, several methods have been introduced to reduce the susceptibility to artefacts caused by metal implants. Among these, the use of ultrashort echo time (UTE) sequences has been proposed [13], an imaging technique that has also been applied for AC in PET/MRI [14]. On the contrary, a preliminary study on the use of UTE-based MRAC in a dental phantom [15] reported on PET and MR signal reduction artefacts caused by dental implants that were similar to the type of artefact we encountered during our evaluation. In the same study, the authors concluded that MRAC artefacts in PET/MRI caused by dental implants are less severe than those in PET/CT and that PET/MRI might thus be of higher diagnostic value for patients with head and neck malignancies [15]. We agree that the common CT streak artefacts do impair the diagnostic quality not only in the location of the dental implant but also in the adjacent tissue, resulting in a decreased confidence of lesion detection in the oral cavity and pharynx. In brief, PET/MRI seems to be less susceptible to the impairment of its morphological component, but this advantage might be accompanied by a loss of PET information. Our evaluation was made with a segmentation-based MRAC method. We did not assess whether the same severity of artefacts could be found when an atlas-based MRAC technique is used. Because atlas-based MRAC methods rely on pattern recognition instead of individual MR pixel values we assume that implanted medical materials will not be the most likely cause of the same severe MRAC artefacts—a hypothesis that requires affirmation in future studies. However, prevention of MRAC artefacts caused by implanted medical materials and development of alternative MRAC techniques less susceptible to this problem is a task that has to be addressed in the process of clinical implementation of PET/MRI. Until then, the information provided by MRAC maps and NAC PET images should be taken into account when reading PET/MRI studies.

This pilot study enrolled a small number of patients. We did not measure the true quantification error caused by MRAC artefacts, for example, by using an AC map obtained from 68 Ge transmission scans. However, by using an individual anatomically matched reference VOI for each artefact site, we believe that we have implemented a reliable reference standard. The delay between ^{18}F-FDG PET/CT and subsequent PET/MRI owing to tracer distribution and elimination might potentially lead to an underestimation or overestimation of the SUV in PET/MRI. Since we did not compare the SUV values between ^{18}F-FDG PET/CT and PET/MRI, we believe that there was no influence of this factor in this particular study. Our preliminary results thus have to be verified by future studies.

CONCLUSIONS

Contrary to PET AC artefacts in PET/CT, which often show as an overestimation of the SUV, MRAC artefacts owing to implanted medical materials in most cases cause a significant underestimation of the ^{18}F-FDG uptake. Being aware of these artefacts reduces the risk of interpretation errors when reading PET/MRI data sets.

REFERENCES

1. Visvikis D, Costa DC, Croasdale I, Lonn AH, Bomanji J, Gacinovic S, et al. CT-based attenuation correction in the calculation of semi-quantitative indices of [^{18}F]FDG uptake in PET. Eur J Nucl Med Mol Imaging 2003;30:344–53. doi: 10.1007/s00259-002-1070-4.
2. Goerres GW, Hany TF, Kamel E, von Schulthess GK, Buck A. Head and neck imaging with PET and PET/CT: artefacts from dental metallic implants. Eur J Nucl Med Mol Imaging 2002;29:367–70.
3. Kamel EM, Burger C, Buck A, von Schulthess GK, Goerres GW. Impact of metallic dental implants on CT-based attenuation

correction in a combined PET/CT scanner. Eur Radiol 2003;13:724–8. doi: 10.1007/s00330-002-1564-2.

4. Bockisch A, Beyer T, Antoch G, Freudenberg LS, Kühl H, Debatin JF, et al. Positron emission tomography/computed tomography—imaging protocols, artifacts, and pitfalls. Mol Imaging Biol 2004;6:188–99. doi: 10.1016/j.mibio.2004.04.006.
5. Hofmann M, Pichler B, Schölkopf B, Beyer T. Towards quantitative PET/MRI: a review of MR-based attenuation correction techniques. Eur J Nucl Med Mol Imaging 2009; 36:S93–104. doi: 10.1007/s00259-008-1007-7.
6. Dixon WT. Simple proton spectroscopic imaging. Radiology 1984; 153:189–94.
7. Hargreaves BA, Worters PW, Pauly KB, Pauly JM, Koch KM, Gold GE. Metal-induced artifacts in MRI. AJR Am J Roentgenol 2011;197: 547–55. doi: 10.2214/AJR.11.7364.
8. Shimamoto H, Kakimoto N, Fujino K, Hamada S, Shimosegawa E, Murakami S, et al. Metallic artifacts caused by dental metal prostheses on PET images: a PET/CT phantom study using different PET/CT scanners. Ann Nucl Med 2009;23: 443–9. doi: 10.1007/s12149-009-0254-4.
9. Goerres GW, Ziegler SI, Burger C, Berthold T, Von Schulthess GK, Buck A. Artifacts at PET and PET/CT caused by metallic hip prosthetic material. Radiology 2003; 226:577–84.
10. Heusner TA, Fronz U, Jentzen W, Verhagen R, Forsting M, Bockisch A, et al. The effect of different chemoembolization materials on CT-based attenuation correction in PET/CT. Rofo 2007;179:1159–65. doi: 10.1055/s-2007-963402.
11. Baek CH, Chung MK, Son YI, Choi JY, Kim HJ, Yim YJ, et al. Tumor volume assessment by 18F-FDG PET/CT in patients with oral cavity cancer with dental artifacts on CT or MR images. J Nucl Med 2008; 49:1422–8. doi: 10.2967/jnumed.108.051649.
12. Rudisch A, Kremser C, Peer S, Kathrein A, Judmaier W, Daniaux H. Metallic artifacts in magnetic resonance imaging of patients with spinal fusion. A comparison of implant materials and imaging sequences. Spine (Phila Pa 1976) 1998;23:692–9.
13. Carl M, Koch K, Du J. MR imaging near metal with undersampled 3D radial UTE-MAVRIC sequences. Magn Reson Med 2013;69:27–36. doi: 10.1002/mrm.24219.
14. Keereman V, Fierens Y, Broux T, De Deene Y, Lonneux M, Vandenberghe S. MRI-based attenuation correction for PET/MRI using ultrashort echo time sequences. J Nucl Med 2010;51: 812–18. doi: 10.2967/jnumed.109.065425.
15. Werner M, Wiegand J, Kupferschläger J, Lois C, Bezrukov I, Pfannenberg C, et al. Do dental implants affect PET/CT and PET/MR image quality equally? Nuklearmedizin 2012;51:V120.